



Rapid Communication: Two-phase Arctic cryosphere patterns associated with delayed Norwegian Sea warming peak during the Last Interglacial

5 Mohamed M. Ezat^{1*}, Pepijn P. Bakker²

¹iC3: Centre for ice, Cryosphere, Carbon and Climate, Department of Geosciences, UiT The Arctic University of Norway, 9037 Tromsø, Norway

²Department of Earth Sciences, Vrije Universiteit Amsterdam, Amsterdam, The Netherlands

10 *Correspondence to:* Mohamed M. Ezat (mohamed.ezat@uit.no)

Abstract. The Last Interglacial (LIG; ~129-117 ka), when global temperatures were comparable to today, provides a valuable testbed for understanding how Arctic cryosphere–ocean interactions may shape regional
15 climate responses. By synthesizing multiproxy records from the Norwegian Sea, North Atlantic, and Southern Ocean, we identify two previously unrecognized phases of delayed Norwegian Sea warming during the early LIG. Phase I (~129-128 ka) was marked by widespread winter sea ice and freshwater input from the retreating Eurasian ice sheets, and was likely associated with large-scale reorganizations of the Atlantic Meridional
20 Overturning Circulation (AMOC). Phase II (during 128-124 ka) featured a localized delay in Norwegian Sea warming peak, likely associated with enhanced Arctic sea-ice melt and freshwater export rather than residual deglacial meltwater. This two-phase framework suggests that sea ice-driven feedbacks, rather than lingering Eurasian ice sheets, were linked to the Phase II delay. Importantly, Phase II does not necessarily imply a
25 synchronous central Arctic cooling, and may instead reflect a localized “warming hole” in the Norwegian Sea. These findings refine the context for the 127 ka Coupled Model Intercomparison Project (CMIP) paleoclimate simulations and further highlight the potential role of Arctic sea ice dynamics in modulating the AMOC and subpolar climate anomalies.

1 Introduction

30 The Atlantic Meridional Overturning Circulation (AMOC) plays an important role in the Earth's climate system by redistributing heat and carbon between hemispheres through the Atlantic basin. Model projections



indicate that the AMOC will weaken as global temperatures rise and Arctic ice continues to melt, with potentially far-reaching impacts on the hydrological cycle, ecosystems, and regional climates (e.g., Masson-Delmotte et al., 2013). However, direct observations of the AMOC are too short to determine whether anthropogenic forcing has
35 already caused a sustained weakening. Consequently, indirect methods, based on AMOC-related observational parameters, have been used to infer longer-term AMOC trends, yet these studies remain inconclusive and strongly debated (e.g., Caesar et al., 2018; Terhaar et al., 2025). A prominent feature potentially linked to the AMOC is the subpolar North Atlantic Warming hole (NAWH), a region south of Greenland and Iceland, where sea surface temperatures have risen slowly, or even cooled, compared to the global mean (e.g., Sevellec et al., 2017; Caesar
40 et al., 2018). While the NAWH has been attributed to AMOC weakening driven by freshwater fluxes from Arctic cryosphere loss (e.g., Sevellec et al., 2017; Caesar et al., 2018), other mechanisms including atmospheric circulation changes have also been implicated (e.g., Keil et al., 2020).

Past warm periods can provide valuable insights for assessing the sensitivity and stability of the AMOC and its associated regional expressions. The Last Interglacial (LIG; ~129-117 ka) is particularly relevant, with
45 global temperatures approximately 0.5-2 °C above preindustrial levels (e.g., Turney and Jones, 2010; Mckay et al., 2011; Hoffman et al., 2017). Although the LIG's warming was driven primarily by enhanced Northern Hemisphere summer insolation rather than anthropogenic CO₂, it still provides a critical test case for understanding ocean-cryosphere feedbacks under warmer-than-preindustrial conditions. Importantly, the LIG
50 climate development was not globally synchronous (e.g., Capron et al., 2014, 2017). In the North Atlantic and the Norwegian Sea, peak warming lagged both the global mean temperature rise and the insolation maximum (Govin et al., 2012; Stone et al., 2016; Capron et al., 2014, 2017; Van Nieuwenhove et al., 2011; Rasmussen et al., 2003; Ezat et al., 2016, 2024). This delay has commonly been attributed to remnant Saalain ice sheets and associated meltwater fluxes that may have weakened the AMOC (e.g., Govin et al., 2012; Stone et al., 2016). While most of the North Atlantic had reached interglacial temperatures by ~127 ka (e.g., Capron et al., 2017), delayed ocean
55 warming may have persisted in the Norwegian Sea until around 124 ka (Van Nieuwenhove et al., 2011; Govin et al., 2012; Rasmussen et al., 2003; Capron et al., 2014; Ezat et al., 2024). The delay in the ocean warming peak in the Nordic seas has also been linked to continued iceberg discharge at high latitudes (e.g., Govin et al., 2012). More recently, enhanced central Arctic sea-ice melt has been proposed as an alternative mechanism for the
60 warming delay (Ezat et al., 2024). It also remains an open question whether the warming delay in the Norwegian Sea implies a synchronous delay in the central Arctic Ocean, with important implications for Arctic sea-ice evolution during the LIG and for forthcoming CMIP paleoclimate simulations.

Here, we reconcile these contrasting interpretations by identifying two previously overlooked phases in the early LIG temperature evolution of the Norwegian Sea, each reflecting a different cryosphere-ocean interaction. We discuss their implications for Arctic sea-ice evolution, AMOC variability, and modern analogues such as the NAWH, and we highlight their relevance for upcoming CMIP paleoclimate simulations.
65

2 Data and Methods

In this study, we synthesize published data based on high-latitude marine sediment records that capture the timing of peak LIG warming in the Norwegian Sea and its relationship to the North Atlantic and Southern Ocean temperature development.



2.1 Selection of sediment cores

Age model uncertainties have direct impacts on spatiotemporal investigations such as this study. Capron et al. (2014, 2017) compiled high-latitude records from both poles and placed them on common timescales. A paleoclimate record represents local information unless a more regional representation is justified (e.g., Neukom et al., 2019). The age models in Capron et al. (2014, 2017) are mostly based on assumptions of synchronous changes in temperature between different ocean areas as well as between ocean and land. Although these assumptions were justified with constrained uncertainties, the assigned uncertainties range from 500 to 2000 years, and up to 4000 years for the Nordic Seas records (Capron et al., 2014), which significantly limits the correlation of spatial changes on millennial or shorter time scales. Further, there are additional unconstrained uncertainties related to limited understanding and potential biases of the proxies used in core chronologies and correlations such as the utility of planktic foraminiferal assemblages as a proxy for SST at low temperatures (e.g., in the Nordic Seas) as well as their potential biases due to, for example, dissolution (see, e.g., Capron et al., 2014; Ezat et al., 2024). Nevertheless, the identification of tephra layer 5e-Low/BAS-IV in some of the Norwegian Sea records and the North Atlantic record ENAM33 provides a unique chronostratigraphic marker and correlation tool between the Nordic Seas and the North Atlantic records (Westgård and Rasmussen, 2001; Abbott et al., 2014; also see Appendix A).

We thus focus on sediment cores MD95-2009, LINK16, and JM11-FI-19PC from the Nordic Seas, where tephra layer 5e-Low/BAS-IV was identified (Westgård and Rasmussen, 2001; Rasmussen et al., 2003; Abbott et al., 2014; Ezat et al., 2016, 2024; Capron et al., 2014) – which is essential for the main objectives of this study.

Although basaltic ash zones were identified in sediment cores HM71-19, HM79-31 (Fronval et al., 1998) and P57-7 (Sjøholm et al., 1991), they clearly differ geochemically from 5e-Low/BAS-IV and a correlation is not possible (Westgård and Rasmussen, 2001). This is particularly important because sediment core HM71-19 was included in the compilation of Capron et al. (2014, 2017), where its basaltic ash zone was assumed to correspond to tephra layer 5e-Low/BAS-IV. In addition to sediment core ENAM33 (in which tephra 5e-Low/BAS-IV was identified from the North Atlantic), representative sea surface temperature records from sediment cores ODP980 (North Atlantic; Oppo et al., 2006) and MD02-2488 (Southern Ocean; Govin et al., 2012) were selected for comparison due to their relatively high temporal resolution (cf. Capron et al., 2014). For core locations, see Table C1 in the Appendices.

2.2 Age models

Chronologies for sediment cores ENAM33, ODP980 (North Atlantic Ocean) and MD02-2488 (Southern Ocean) follow Capron et al. (2014). In brief, the AICC2012 ice core chronology (Bazin et al., 2013; Veres et al., 2013) was used as a reference, assuming that SST changes in the Southern Ocean and the North Atlantic occurred simultaneously with air temperature variations over inland Antarctica and Greenland, respectively (Appendix A; for details see Govin et al., 2012; Capron et al., 2014). For the Nordic Seas records (MD95-2009, LINK16, JM11-FI-19PC), we adopted the slightly modified approach of Capron et al. (2014) in Ezat et al. (2024), in which Nordic Seas sediment cores were aligned to ENAM33 using five tie points, including the tephra layer 5e-Low/BAS-IV (see Appendix A). Age uncertainties range from 500 to 4000 years (Capron et al., 2014; see Appendix A).



110 3. Results and Discussion

3.1 Two distinct phases of delayed peak warming in the Norwegian Sea during the LIG

Figure (1) compares Summer Sea Surface Temperature (SSST) records from the Southern Ocean, the North Atlantic Ocean as well as SSST-, sea ice- and freshwater dynamics- related records from the Norwegian Sea, spanning the latest stage of penultimate deglaciation (132-129 ka) and most of the LIG (129-120 ka). The 115 records reveal two distinct delay phases of the LIG warming peak in the Norwegian Sea. Phase I (~129-128 ka) is characterized by a delayed warming peak in both the North Atlantic and the Norwegian Sea relative to the Southern Ocean (Fig. 1). During this phase, winter sea ice was extended to the southernmost Nordic Seas (Ezat et al., 2024; Fig. 1), and meltwater of continental origin persisted, evidenced by elevated Ba/Ca (Figure 1, Ezat et al., 2024) and Ice Rafted Debris (IRD; Figure 1; e.g., Rasmussen et al., 2003), and lower seawater $\delta^{18}\text{O}$ (Ezat et al., 2016; Ezat et al., 2024), likely sourced from Eurasian ice sheets (cf. Govin et al., 2012). These freshwater 120 fluxes could have contributed to significant changes in the AMOC (Govin et al., 2012; Stone et al., 2016). Phase II (~127.5-124) in which the North Atlantic SSST reached its LIG peak (e.g., Capron et al., 2014) while Norwegian Sea SSST indicates a further delay where sea surface conditions were colder (Rasmussen et al., 2003; Hoff et al., 2019; Ezat et al., 2016; Van Nieuwenhove et al., 2011) and possibly fresher (Ezat et al., 2024) than the 125 later part of the LIG.

Unlike Phase I, relatively low planktic foraminiferal Ba/Ca (similar to the values of the later part of the LIG), relatively higher seawater $\delta^{18}\text{O}$ and absence of IRD suggest that hypothesized freshwater did not originate from Eurasian ice sheets, icebergs or continental runoff (Ezat et al., 2024). Instead, Ezat et al. (2024) suggested that the early LIG northern insolation maximum might have coincided with a meltwater flux derived from 130 enhanced melting of Arctic sea ice that reached the Nordic Seas. This meltwater might have altered Nordic Seas deep water formation and limited oceanic heat transport into the region, further delaying Interglacial warmth in the Norwegian Sea. Phase I thus represents deglacial ice sheet–ocean interactions, whereas Phase II likely reflects ocean–sea ice interactions under warmer-than-preindustrial conditions.

The recognition of these two phases helps explain why earlier studies did not distinguish between them, 135 as most previous compilations relied primarily on planktic foraminiferal assemblages to reconstruct SSST in the Nordic Seas (e.g., Capron et al., 2014, 2017). Planktic foraminiferal assemblages do not suggest changes in SSST between Phases I and II (Fig. 1c), which likely contributed to the lack of distinction between the two delay phases. However, diatom assemblages (Hoff et al., 2019), another proxy for SSST, suggest that while the warming peak was delayed in the Norwegian Sea until the end of Phase II at ~124 ka, sea surface temperature 140 started to increase during Phase II relative to Phase I (Fig. 1c; Appendix B). Further, sea ice proxies (Ezat et al., 2024) indicate that while extensive sea ice extended to the southern Norwegian Sea during Phase I, the Norwegian Sea was sea ice free all year-round during Phase II. Thus, the consideration of a multiproxy approach to reconstruct Nordic Seas SSST as well as the recently published additional data on sea ice and freshwater 145 source changes facilitated the identification of the two phases. The absence of changes in planktic foraminifera assemblages between Phase I and Phase II (compared to sea ice proxies and other SSST-related fossil assemblages) can be partly related to calcium carbonate preservation as Phase II is characterized by the lowest calcium carbonate content in Norwegian Sea sediments (e.g., Fig. 1f). In addition, what is defined here as Phase I of the Last Interglacial was considered part of the penultimate deglaciation in several previous studies (e.g.,



150 Rasmussen et al., 2003; Ezat et al., 2024), further obscuring a distinction between the two phases. As a result, Ezat et al. (2024) discussed Arctic sea-ice melt as a potential alternative mechanism for the delayed warming of both the North Atlantic and the Norwegian Sea, rather than lingering Eurasian ice-sheet influence. By synthesizing regional records, we show that this sea-ice–driven mechanism is more consistently associated with a localized warming delay in the Norwegian Sea during Phase II, rather than with the broader North Atlantic delay observed during Phase I.

155 Age model uncertainties have direct impacts on spatiotemporal investigations such as this study, and the assigned age model uncertainties of 500 to 4000 years, limit precise correlation on millennial or shorter timescales (see Methods and Appendix A). Yet, the tephra layer 5e-Low/BAS-IV provides a robust chronostratigraphic marker between the Nordic Seas and the North Atlantic records, providing confidence in identifying Phase II of the LIG peak warming delay in the Norwegian Sea, relative to the North Atlantic (Fig.1).
160 Nevertheless, the absolute age this tephra layer remains uncertain, limiting precise dating of Phase II as well as how long it lasted.

3.2 Implications for LIG Arctic sea ice and ocean circulation changes

165 The Phase II configuration identified here implies that within the time interval ~128–124 ka, the Norwegian Sea experienced cold and potentially fresh surface conditions compared to the later part of the LIG and the Holocene, while the wider North Atlantic had already attained interglacial temperatures. A key question is whether this delay reflects synchronous cooling in the central Arctic Ocean. Equilibrium simulations centered around 127 ka were considered as the most suitable for examining the impact of a stronger orbital forcing relative to the preindustrial conditions and are thus assumed to likely capture the interval most representative of enhanced
170 Arctic sea-ice retreat and its influence on the AMOC (e.g., Otto-Bliesner et al., 2017). Also, models that achieve seasonally ice-free Arctic summers during the LIG (e.g., Guarino et al., 2020) do so only at the summer insolation peak (i.e., not later in the LIG). Thus, whether the Norwegian Sea warming delay during Phase II implies a synchronous central Arctic cooling has important implications for understanding Arctic sea-ice changes during the LIG and the applicability of 127 ka simulations for studying enhanced Arctic sea ice melt and
175 associated sea ice-AMOC interactions during the LIG.

180 Direct constraints on the contemporaneous state of the central Arctic Ocean remain sparse due to chronological uncertainties and contrasting proxy interpretations. For example, biomarker-based reconstructions suggest perennial sea ice cover in the central Arctic Ocean (Stein et al., 2017), whereas the presence of subpolar planktic foraminifera in sediments attributed to the same interval has been used to infer sea ice-free summers (Vermassen et al., 2023). Moreover, several of these central Arctic records have recently been re-evaluated, and their LIG age assignments have been questioned (Razmjooei et al., 2023).

185 Freshwater source proxies suggest that the Norwegian Sea cooling during Phase II is consistent with enhanced Arctic sea ice melt and southward export of meltwater, which may have reduced open-ocean convection and limited northward oceanic heat transport (Ezat et al., 2024; Figure 1). These findings suggest that the delayed Norwegian Sea warming in Phase II does not necessarily imply a synchronous delay in the central Arctic. Instead, Phase II configuration here agrees more with higher sea-surface temperatures and reduced sea-ice cover in the central Arctic, which also appear more consistent with both model simulations (Guarino et al., 2020) and Greenland ice-core evidence (Dahl-Jensen et al., 2013) for elevated temperatures.



This updated framework supports the use of 127 ka as a target interval for CMIP/PMIP equilibrium and 190 transient simulations exploring potentially reduced Arctic sea ice and its interactions with radiative forcing, ocean circulation, and regional climate. Viewed in this context, delayed warming in the Norwegian Sea during Phase II can be considered a “warming hole”. This also offers a useful case study, where Arctic sea-ice decline and 195 freshwater export may contribute to regional cooling anomalies in the subpolar North Atlantic, the so-called NAWH (e.g., Caesar et al., 2018; Keil et al., 2020), although the spatial location of the warming hole differs. For example, recent reconstructions of subpolar ocean temperatures during the Holocene (at ~5.8–4.8 ka and after 200 ~2.2 ka) show that central-western North Atlantic SSTs rapidly cooled while northwest Europe summer temperatures increased, and eastern North America cooled (Shuman et al., 2025). This has been interpreted as a warming hole pattern linked to reductions in deep ocean overflow south of Iceland. Future data–model integration studies should investigate whether similar processes operated during the early LIG.

4 Summary and Conclusions

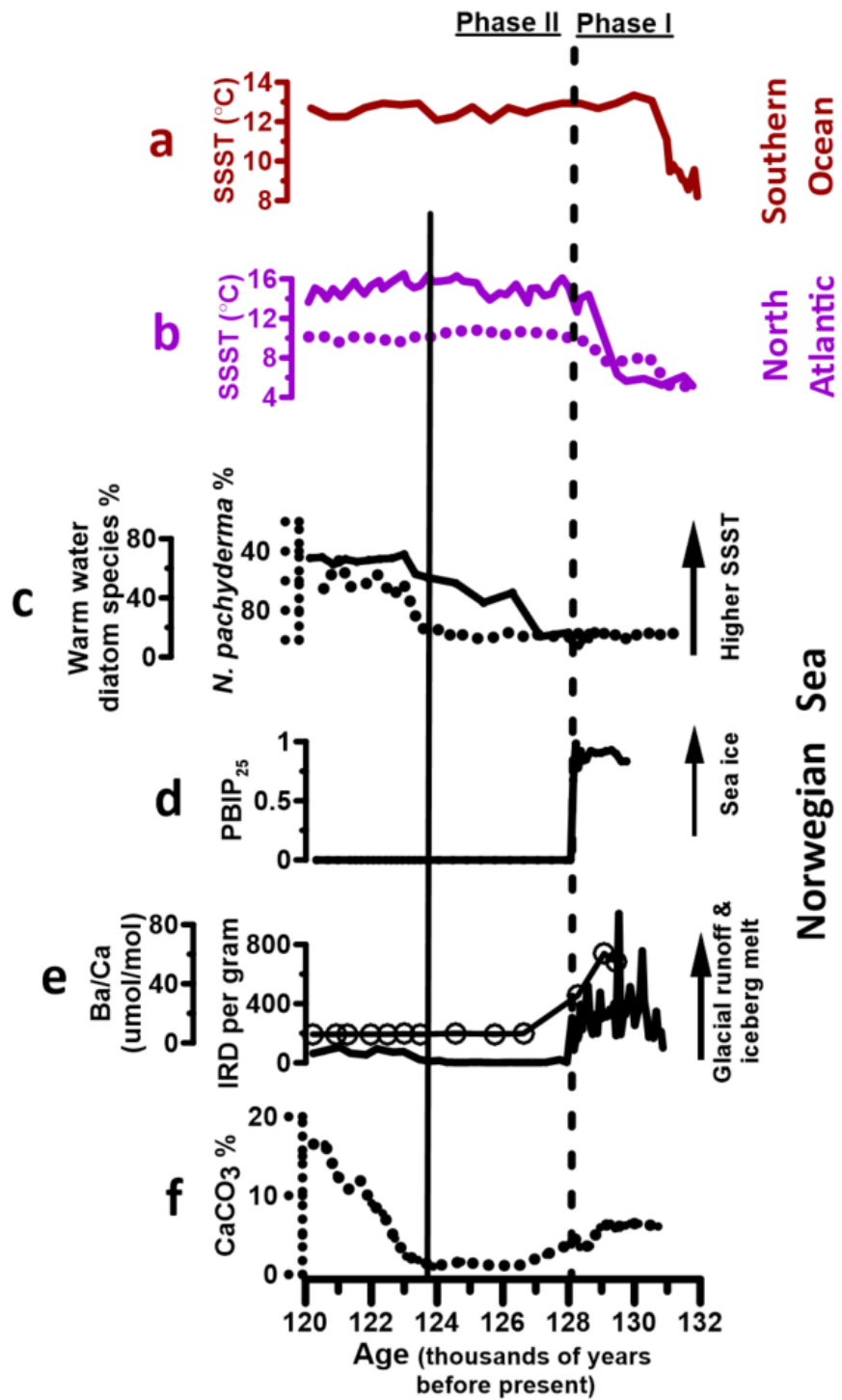
Comparison of multiproxy records from the Norwegian Sea with SST records from the Southern Ocean and North Atlantic reveals two previously unrecognized phases of delayed peak ocean warming during the early 205 LIG. Phase I (~129–128 ka) was marked by a concurrent delay in both North Atlantic and Norwegian Sea warming relative to the Southern Ocean, accompanied by extensive winter sea ice reaching the southern Nordic Seas and persistent freshwater input of continental origin from melting Eurasian ice sheets. These meltwater fluxes likely contributed to a large-scale reorganization of the AMOC. In contrast, Phase II (~128–124 ka) was characterized by a further, but localized, delay in peak interglacial warmth in the Norwegian Sea, though it was 210 sea-ice free all year round. The absence of continental meltwater indicators points to enhanced melting of central Arctic sea ice, producing freshwater fluxes that may have reduced or altered convection in the Nordic Seas and delayed regional oceanic warming. Building on Ezat et al. (2024), who proposed Arctic sea-ice melt and 215 freshwater export as key mechanisms during early LIG, our synthesis demonstrates that this process represents a distinct second phase of delayed warming, separate from the deglacial meltwater influence of Phase I. The integration of multiproxy evidence for Norwegian Sea SST, sea-ice cover, and freshwater sources, in comparison to North Atlantic and Southern Ocean SST records, was essential for distinguishing these two mechanisms. Recognizing this two-phase structure clarifies that Phase II was not a lingering deglacial signal but a sea ice-ocean-climate feedback process operating under warmer-than-preindustrial conditions.

We also suggest that the delay of the Norwegian Sea warming peak in Phase II may not imply a 220 synchronous warming delay in the central Arctic Ocean. Instead, this configuration of Phase II may reflect a “warming hole”, occurring while most of the North Atlantic and central Arctic Ocean experienced interglacial warmth – a feature potentially similar in mechanism, though not location, to the modern NAWH. This refined framework has direct implications for the design and interpretation for the forthcoming LIG simulations of the 225 CMIP paleoclimatic experiments. It also provides a more nuanced context for interpreting the 127 ka equilibrium experiments and underscores the critical role of Arctic sea ice dynamics in modulating AMOC strength and subpolar climate anomalies – both during past warm periods and in our rapidly warming future.

Figures



230 **Figure 1. Norwegian Sea records of summer sea surface temperature (SSST) and meltwater sources, compared to SSST records from the North Atlantic Ocean and the Southern Ocean.** (a) Southern Ocean SSST based on sediment core MD02-2488 (46.47°S, 88.02°E; Govin et al., 2012). (b) North Atlantic SSST based on sediment cores ODP-980 (55.49°N, 14.70°W; solid line; Oppo et al., 2006) and sediment core ENAM33 (61.16°N, 11.01°W; dashed line; Rasmussen et al., 2003; Capron et al., 2014) – indicating a delay in the LIG peak warmth in
235 the North Atlantic compared to the Southern Ocean (**Phase I**). (c) Records of relative changes in SSST in the Norwegian Sea (~62.5°N, 3°W): relative abundance of warm water-indicating diatom species (solid line; Hoff et al., 2019); and relative abundance of the cold-water planktic foraminiferal species *Neogloboquadrina pachyderma* (dashed line; Rasmussen et al., 2003) – illustrating a further delayed phase in the LIG warming peak in the Norwegian Sea, compared to the North Atlantic (**Phase II**). (d) Sea ice index $P_B IP_{25}$, calculated based on the sea
240 ice biomarker IP_{25} (a C₂₅ Isoprenoid Lipid) and phytoplankton indicators (Ezat et al., 2024) – indicating the presence of winter and spring sea ice in the southern Norwegian Sea during **Phase I** of the warming delay and open ocean conditions all year round during **Phase II** of the warming delay (Ezat et al., 2024). (e) Glacier and iceberg meltwater proxies: Ba/Ca measured in *N. pachyderma* (Ezat et al., 2024), which serves as a proxy of freshwater of continental origin (open circles and solid line); and content of Ice Rafted Debris (IRD; Rasmussen et al., 2003), which is a proxy for iceberg melting (solid line), showing no indication of freshwater of continental origin during **Phase II** of the warming delay, in contrast to **Phase I** of delayed warming. (f) Calcium carbonate (CaCO₃) content (Hoff et al., 2019), which is an indicator of CaCO₃ flux and/or preservation. Norwegian Sea records are based on sediment cores JM11-FI-19PC (solid lines) and MD95-2009 (dashed lines). **Vertical solid line** highlights the position of tephra layer 5e-Low/BAS-IV in the Norwegian Sea records and the North Atlantic record ENAM33, which
245 provides a unique chronostratigraphic marker and correlation tool between the Norwegian Sea and North Atlantic records (Capron et al., 2014; Rasmussen et al., 2003; Ezat et al., 2016) i.e., providing confidence in the identification of **Phase II** of the LIG warming delay. **Vertical dashed line** defines the boundary between **Phase I** of delayed warming of the North Atlantic (and the Norwegian Sea) with respect to the Southern Ocean and **Phase II** of delayed warming in the Norwegian Sea with respect to the North Atlantic Ocean.





Appendices



Appendix A: Age models and associated uncertainties

For North Atlantic (ENAM33, ODP980) and Southern Ocean (MD02-2488) sediment cores, Capron et al. (2014) used the AICC2012 ice core chronology (Bazin et al., 2013; Veres et al., 2013) as the reference timescale, assuming that SST changes in the Southern Ocean and the North Atlantic occurred simultaneously with air temperature variations over inland Antarctica and Greenland, respectively (For details see Govin et al., 2012; Capron et al., 2014). In this chronology framework, the North Atlantic sediment cores were aligned to the AICC2012 ice-core timescale by synchronizing their SST variations with Greenland NGRIP $\delta^{18}\text{O}$ (as a proxy for Greenland air temperature) record until 122 ka where the NGRIP record ends. Prior to 122 ka, the synchronization is based on the timing of globally synchronous methane increases, relying on the well-established observation that, during abrupt climate events of the last glacial period, North Atlantic SSTs nearly rose in step with Greenland air-temperature changes and rapid methane increases in the atmosphere (e.g., Bond et al., 1993; Chappellaz et al., 1993; Govin et al., 2012; Capron et al., 2014).

For the Nordic Seas records (MD95-2009, LINK16, JM11-FI-19PC), we adopted the slightly modified approach of Capron et al (2014) as implemented in Ezat et al. (2024), in which Nordic Seas sediment cores were aligned to core ENAM33 from the northern North Atlantic, using five tie points: (1) the onset of the deglacial decline in benthic $\delta^{18}\text{O}$, dated at 138.2 ± 4 ka (Capron et al., 2014); (2) a common major change in the benthic foraminiferal assemblage composition of replacing what is called “Atlantic Species” with interglacial-indicating benthic species, which was used as a marker of the onset of ocean convection and strengthened southward export of deep-water across the Greenland Scotland Ridge (Rasmussen et al., 2003). This event was dated at 128 ± 1.5 ka (Capron et al., 2014), and coincides with a remarkable increase in benthic $\delta^{18}\text{O}$ in the Norwegian Sea sediment cores; benthic $\delta^{18}\text{O}$ is thus used instead in cores where benthic foraminiferal assemblages are not studied (Ezat et al., 2024); (3) the tephra layer 5e-Low/BAS-IV, identified in both ENAM33 and the studied Nordic Seas records (Abbot et al., 2014; Rasmussen et al., 2003; Ezat et al., 2016) and was dated to 123.7 ± 2 ka (Capron et al., 2014); (4) a pronounced cooling in Nordic Seas SSSTs (as seen in the changes in the abundance of the polar planktic foraminifer *N. pachyderma* and its $\delta^{18}\text{O}$ records) corresponding to an abrupt temperature decrease in the NGRIP ice-core record at 116.7 ± 2 ka, interpreted as the termination of the LIG; and (5) core JM11-FI-19PC does not capture the full penultimate deglaciation; its basal section was assigned an age of ~ 130 ka by correlating its planktic and benthic $\delta^{18}\text{O}$ records with those of MD95-2009 and LINK 16 (Ezat et al., 2024). The identification of tephra layer 5e-Low/BAS-IV in the Norwegian Sea records and the North Atlantic record ENAM33 provides a unique chronostratigraphic marker and correlation tool between these records (Westgård and Rasmussen, 2001; Abbot et al., 2014), providing confidence in identifying Phase II of the LIG warming delay in the Norwegian Sea, relative to the North Atlantic. While the absolute age this tephra layer is uncertain, limiting precise dating of Phase II as well as how long it lasted, it is most likely that Phase II started sometime between 129 and 126.5 ka (Capron et al., 2014). This implies that the characteristics of Phase II are relevant to the 127 ka experiments in the CMIP paleoclimate simulations.

In brief, the age models of the North Atlantic (ENAM33, ODP980) and Southern Ocean (MD02-2488) sediment cores follow Capron et al. (2014), whereas the age models of the Norwegian Sea sediment cores (MD95-2009, LINK16, JM11-FI-19PC) are based on the slightly modified approach of Capron et al. (2014) described in Ezat et al. (2024).



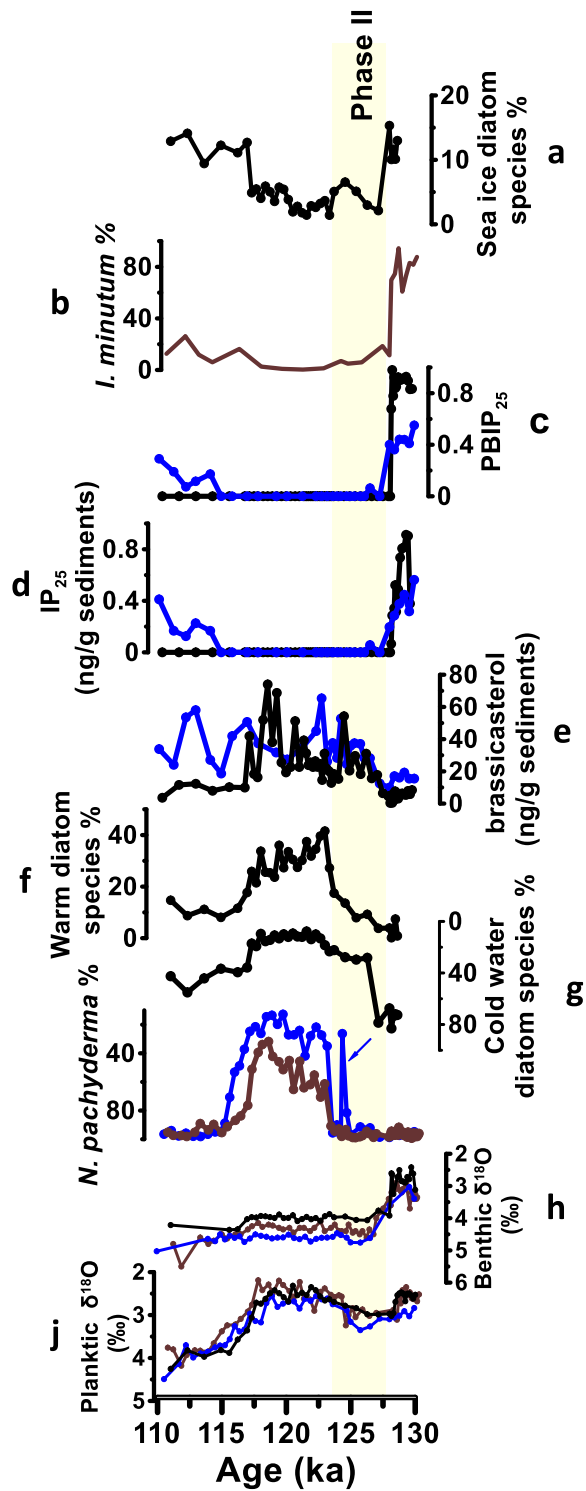
305

Appendix B – Figure B1: Summer sea surface temperature and sea-ice records from the Norwegian Sea.

Black, blue and brown colors refer to data from sediment cores JM11-FI-19PC, LINK16 and MD95-2009, respectively. **Sea ice proxies:**

(a) Relative abundance of sea-ice indicating diatom species (Hoff et al., 2019); **(b)** Relative abundance of the dinocyst sea-ice species *Islandinium minutum* (Van Nieuwenhove et al., 2011); **(c)** Sea-ice index PBIP25 from two sediment cores (Ezat et al., 2024); **(d)** Concentration of IP25 (a C25 Isoprenoid Lipid) (Ezat et al., 2024); and **(e)** Concentration of brassicasterol (Ezat et al., 2024). Temperature proxies: **(f)** Relative abundance of warm water-indicating diatom species (Hoff et al., 2019); **(g)** Relative abundance of cold water-indicating diatom species (Hoff et al., 2019); and **(h)** Relative abundance of the polar planktic foraminiferal species *Neogloboquadrina pachyderma* (Rasmussen et al., 2003; Abbott et al., 2014). **(i)** Benthic foraminiferal $\delta^{18}\text{O}$ (Rasmussen et al., 2003; Ezat et al., 2016, Ezat et al., 2024). **(j)** Planktic foraminiferal $\delta^{18}\text{O}$ (Rasmussen et al., 2003; Ezat et al., 2016, Ezat et al., 2024). Note the inverted y-axis in plots (g), (h), (i) and (j). Blue arrows refer to an interval (peak) in core LINK16 that is likely affected by bioturbation (for details, see Supplemental Figure 1 in Ezat et al., 2024).

320





Appendix C – Table C1. Locations of the sediment cores discussed in this study.

Core Name	Latitude (N)	Longitude (E)	Water Depth (m)
MD95-2009	62.74	-4	1027
JM11-FI-19PC	62.82	-3.87	1179
LINK 16	62.60	-3.52	773
ENAM-33	61.27	-11.16	1217
ODP980	55.8	-14.11	2168
MD02-2488	-46.48	88.02	3420

325 Data availability

This study is based exclusively on previously published datasets, all of which are publicly available in the original publications cited throughout the manuscript

Author Contributions

MME conceived the study and wrote the first draft. MME and PPB designed the study and wrote the manuscript.

330

Competing interests

The authors declare no competing interests.

Acknowledgement

335 MME is supported by Tromsø Forskningsstiftelse, project number A31720 (the ARCLIM project), and is also part of the Centre of Excellence iC3 (grant number 332635) and the ERC Synergy Project i2B (grant number 101118519). We thank Emilie Capron for providing easy access to published data and for valuable discussions. We also thank Peter Abbott for expert advice on tephrostratigraphy.



340 References

Abbott, P. M. et al. Re-evaluation and extension of the Marine Isotope Stage 5 tephrostratigraphy of the Faroe Islands region: The cryptotephra record. *Palaeogeogr., Palaeoclimatol., Palaeoecol.* **409**, 153–168 (2014).

Bazin, L., et al. 2013. An optimized multi-proxy, multi-site Antarctic ice and gas orbital chronology (AICC2012): 345 120e800 ka. *Clim. Past* **9**, 1715e1731.

Caesar, L., et al. (2018). Observed fingerprint of a weakening Atlantic Ocean overturning circulation. *Nature*, **556**, 191–196.

Capron, E. et al. (2014). Temporal and spatial structure of multi-millennial temperature changes at high latitudes during the Last Interglacial. *Quat. Sci. Rev.* **103**, 116–133

350 Capron, E., Govin, A., Feng, R., Otto-Bliesner, B. L., & Wolff, E. W. (2017). Critical evaluation of climate syntheses to benchmark CMIP6/PMIP4 127 ka Last Interglacial simulations in the high-latitude regions. *Quaternary Science Reviews*, **168**, 137–150.

Chappellaz, J., Blunier, T., Raynaud, D., Barnola, J.-M., Schwander, J., Stauffer, B., 1993. Synchronous changes in atmospheric CH₄ and Greenland climate between 40 kyr and 8 kyr BP. *Nature* **366**, 443e445.

355 Dahl-Jensen et al. (2013) Eemian interglacial reconstructed from a Greenland folded ice core. *Nature*, **489**–494.

Ezat, M. M., Fahl, K., & Rasmussen, T. L. (2024). Arctic freshwater outflow suppressed Nordic Seas overturning and oceanic heat transport during the Last Interglacial. *Nature Communications*, **15**(1), 8998.

Ezat, M. M., Rasmussen, T. L. & Groeneveld, J. (2016) Reconstruction of hydrographic changes in the southern 360 Norwegian Sea during the past 135 kyr and the impact of different foraminiferal Mg/Ca cleaning protocols. *Geochem., Geophysics, Geosystems* **17**, 3420–3436.

Fronval, T., Jansen, E., Haflidason, H., Sejrup, H.-P., 1998. Variability in surface and deep water conditions in the Nordic seas during the last interglacial period. *Quat. Sci. Rev.* **17**, 963e985.

Govin, A., et al. (2012). Persistent influence of ice sheet melting on high northern latitude climate during the early Last Interglacial. *Climate of the Past*, **8**(2), 483–507.

365 Guarino, M. V., et al. (2020). Sea-ice-free Arctic during the Last Interglacial supports fast future loss. *Nature Climate Change*, **10**(10), 928–932.

Hoff, U., Rasmussen, T. L., Meyer, H., Koç, N. & Hansen, J. (2019). Palaeoceanographic reconstruction of 370 surface-ocean changes in the southern Norwegian Sea for the last ~130,000 years based on diatoms and with comparison to foraminiferal records. *Palaeogeogr., Palaeoclimatol., Palaeoecol.* **524**, 150–165.

Hoffman, J. S., Clark, P. U., Parnell, A. C., & He, F. (2017). Regional and global sea-surface temperatures during the last interglaciation. *Science*, **355**(6322), 276–279.

Keil, P., et al. (2020). Multiple drivers of the North Atlantic warming hole. *Nature Climate Change*, **10**, 667–671.

Masson-Delmotte, V. et al. in Climate Change 2013: The Physical Science Basis. Contribution of Working Group 375 I to the Fifth Assessment Report of the Intergovernmental Panel on Climate Change Ch. 5 (eds Stocker, T. F. et al.) 383–464 (Cambridge Univ. Press, Cambridge, 2013).

McKay, N.P., Overpeck, J.T., Otto-Bliesner, B.L., 2011. The role of ocean thermal expansion in Last Interglacial sea level rise. *Geophys. Res. Lett.* **38**

Neukom, R., Steiger, N., Gómez-Navarro, J. J., Wang, J., & Werner, J. P. (2019). No evidence for globally 380 coherent warm and cold periods over the preindustrial Common Era. *Nature*, **571**(7766), 550–554.

Oppo, D. W., McManus, J. F., & Cullen, J. L. (2006). Evolution and demise of the Last Interglacial warmth in the subpolar North Atlantic. *Quaternary Science Reviews*, **25**(23–24), 3268–3277.



Otto-Bliesner, B. L., et al. (2017). The PMIP4 contribution to CMIP6—Part 2: Two interglacials, scientific objective and experimental design for Holocene and Last Interglacial simulations. *Geoscientific Model Development*, 10(11), 3979–4003.

385 Rasmussen, T. L., Thomsen, E., Kuijpers, A. & Wastegård, S. (2003) Late warming and early cooling of the sea surface in the Nordic seas during MIS 5e (Eemian Interglacial). *Quat. Sci. Rev.* 22, 809–821.

Rasmussen, T. L., Thomsen, E., Kuijpers, A., & Wastegård, S. (2003). Late warming and early cooling of the sea 390 surface in the Nordic seas during MIS 5e (Eemian Interglacial). *Quaternary Science Reviews*, 22(8-9), 809–821.

Razmjooei, M. J. et al. (2023). Revision of the Quaternary calcareous nannofossil biochronology of Arctic Ocean sediments. *Quaternary Science Reviews*, 321, 108382.

Sévellec, F., et al. (2017). Arctic sea-ice decline weakens the Atlantic meridional overturning circulation. *Nature Climate Change*, 7, 604–610.

395 Shuman, B. N., & Stefanescu, I. C. (2025). North American “warming holes” and European heat during abrupt Holocene cooling events in the Atlantic. *Nature Communications*, 16(1), 9057.

Sjøholm, J., Sejrup, H. P., & Furnes, H. (1991). Quaternary volcanic ash zones on the Iceland Plateau, southern Norwegian Sea. *Journal of Quaternary Science*, 6(2), 159–173.

Stein, R., et al. (2017) Arctic Ocean sea ice cover during the penultimate glacial and the last interglacial. *Nature 400 Communications*.

Stone, E. J., et al. (2016). Impact of meltwater on high-latitude early Last Interglacial climate. *Climate of the Past*, 12, 1919–1932.

Terhaar, J., Vogt, L., & Foukal, N. P. (2025). Atlantic overturning inferred from air-sea heat fluxes indicates no decline since the 1960s. *Nature Communications*, 16(1), 222.

405 Turney, C.S.M., Jones, R.T., 2010. Does the Agulhas Current amplify global temperatures during super-interglacials? *J. Quat. Sci.* 25 (6), 839e843.

Van Nieuwenhove, N. et al. (2011) Evidence for delayed poleward expansion of North Atlantic surface waters during the last interglacial (MIS 5e). *Quat. Sci. Rev.* 30, 934–946.

Veres, D. et al. The Antarctic ice core chronology (AICC2012): an optimized multi-parameter and multi-site 410 dating approach for the last 120 thousand years. *Clim* 9, 1733–1748 (2013).

Vermassen, F. et al. (2023) A seasonally ice-free Arctic Ocean during the last interglacial. *Nature Geoscience*.

Wastegård, S., & Rasmussen, T. L. (2001). New tephra horizons from Oxygen Isotope Stage 5 in the North Atlantic: correlation potential for terrestrial, marine and ice-core archives. *Quaternary Science Reviews*, 20(15), 1587–1593.